Supplementary Information

Deactivation, reactivation and super-activation of Fe-N/C oxygen reduction electrocatalysts: gas sorption, physical and electrochemical investigation using NO and O_2

Paul Boldrin[b], Daniel Malko[a], Asad Mehmood[a], Ulrike I. Kramm[c], Stephen Paul[c], Natascha Weidler[c], Anthony Kucernak[a,*]

[a] Department of Chemistry, Imperial College London, London UK

[b] Department of Earths Science and Engineering, Imperial College London, London UK

[c] FG Katalysatoren und Elektrokatalysatoren, Technische Universität Darmstadt, Darmstadt, Germany

Contents

S1. Details of synthesis of catalyst

Fe- N/C and N/C

The catalyst **Fe-N/C** was synthesized by dissolving 1.0 g (6.4 mmol) of 1,5-Diaminonaphthalene (97%, Alfa Aesar), 1.0 g (4.4 mmol) of $(NH_4)_2S_2O_8$ (98%, Sigma-Aldrich) and 35.6 mg of $FeCl_2*4H_2O$ (99%, Sigma-Aldrich) in 250 mL of ethanol (absolute, VWR). The solution was stirred for 24h at room temperature. The solvent was then removed with a rotary evaporator. When dry, the resulting residue was transferred to an alumina boat (11cm long by 2cm wide by 1 cm deep, approximately 10mL of volume capacity) and heat treated at 950 °C for 2h, after reaching the end temperature, in a tube (quartz) furnace (Carbolite) at a heating rate of 20 °C/min. This heat treatment was performed in an inert atmosphere, under a continuous flow of nitrogen (50 ccm). After cooling down under nitrogen, the resulting material was removed from the quartz boat and refluxed in 0.5M H_2SO_4 for 8h, in order to remove any soluble metal phases. The material was then filtered and dried. The dried powder was then subjected to a second heat treatment at 900 °C for 2h after reaching the target temperature at a heating rate of 20 °C/min under nitrogen and allowed to cool as above. The resulting powder was then ready to use. The catalyst **N/C** was synthesized in the same way without the addition of the metal salt.

Carbon black (Ketjen Black EC600-JD)

The Carbon Black was treated with 1M HCl and washed with DI water in order to remove iron impurities.

S2. Properties of catalyst

BET analysis of Fe-N/C, N/C catalysts and Ketjen Black EC600-JD.

The Brunauer–Emmett–Teller (BET) equation was used to extract the surface area. Microporous and external surface area (SA) were determined from the t-plot using the Broekhoff-DeBoer thickness equation. Samples were thoroughly degassed and dried overnight at 300 °C under nitrogen prior to the measurement.

Table S1 ¦ BET Parameters of catalysts

Catalyst	Microporous SA / $m^2 g^{-1}$	External SA / $m^2 g^{-1}$	Total SA / $m^2 g^{-1}$
Fe-N/C	421	110	531
N/C	550	101	651
Ketjen Black EC600-JD[1]	592	824	1416

S3. Deconvolution of TPD peaks to obtain NO adsorption quantities

Deconvolution of peaks was carried out using the "fit peaks" routine in the peak analyser in Origin Pro 2017 on time resolved data (rather than temperature resolved). No baseline correction was necessary. Two peaks were fitted corresponding to the low and high temperature peaks. The low temperature peak was fitted as a log normal peak, while the high temperature peak was fitted as a Gaussian peak. The reason for this is that the high temperature peak is a second order desorption which should present as a Gaussian peak, while it was assumed that the low temperature peak was zero or first order which should present as a log normal peak.

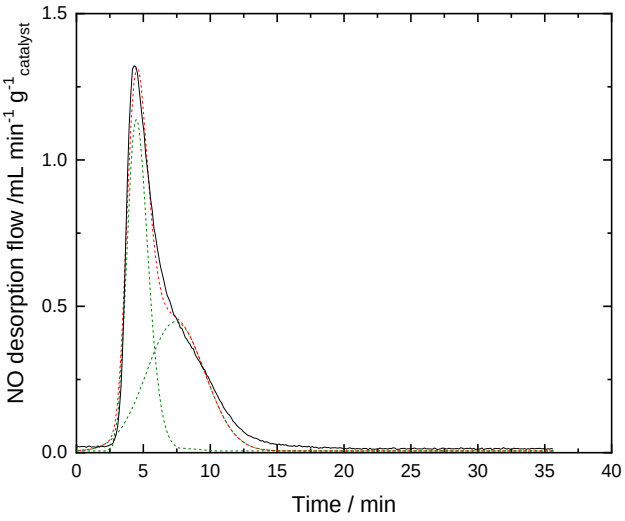

Figure S1 ¦ Temperature programmed desorption curve for NO adsorbed onto Fe-N/C (black) showing fitted low and high temperature peaks (dotted green lines) and overall fit (dotted red line)

Deconvolution of the peaks, and plotting $\ln(-d\theta_{peak}/dt)-n\ln(\theta_{peak})$ against 1/T for the deconvoluted high temperature peak, where θ is the coverage, n is the kinetic order of desorption and T is the temperature, should give a straight line when the correct order of the reaction is used, **Figure S2**. The activation energy can be calculated from the gradient and the kinetic order of desorption deduced by using different values of n, with the value which gives a straight line through the region of the peak maximum corresponding to the correct order of desorption[2]. Data is plotted for n=1, and n=2, with only the latter giving a straight line. The activation energy of the high temperature peak is found to be 46.1 kJ mol^{-1} with n=2, which is indicative of a relatively weak chemisorption.

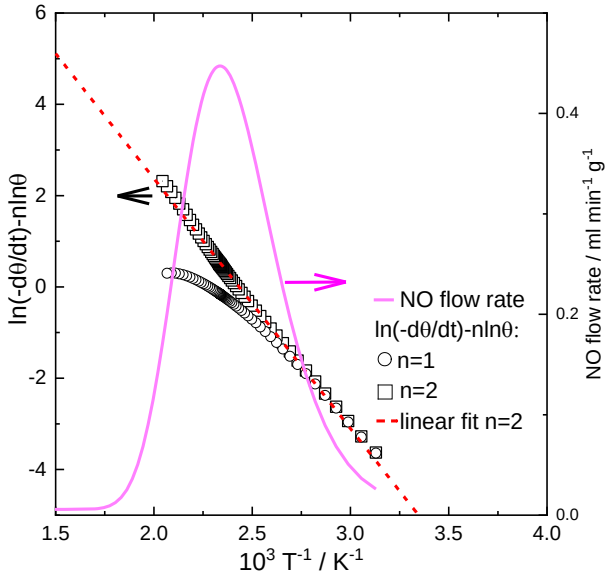

Figure S2 ¦ Estimation of reaction order for desorption and resultant activation energy

S4. Details of electrochemical measurements

Measurements were conducted with a Rotating Ring Disk Electrode (Pine Instruments, model AFE6R1AU, with a mirror polished glassy carbon disk and rotator model AFMSRCE), the catalyst was deposited on the glassy carbon disk as per literature procedure.[3, 4] RDE results were obtained at a disk rotation rate of 1600 RPM. The ink utilised consisted of 1wt% catalyst in a 1:1 volume ratio mixture of IPA (VWR):H_2O (MilliQ 18.2 MΩ cm) with a Nafion to catalyst weight ratio of 1:1. This composition was found to give a uniform catalyst layer. A custom made three compartment electrochemical glass cell was used. The reference electrode was ionically connected to the main compartment of the electrochemical glass cell via a Luggin-Haber-Capillary. For measurements in 0.5M H_2SO_4, a RHE (GaskatelHydroFlex) was used. For measurements in the higher pH electrolytes a saturated calomel electrode SCE (VWR) was used and the potentials with respect to the RHE scale were determined by measuring the change from hydrogen evolution to hydrogen oxidation in the respective H_2-saturated electrolyte on a platinized platinum wire. A glassy carbon rod was used as counter electrode and ionically connected to the main compartment of the glass cell through a porous frit. Glassy carbon was used instead of Pt in order to avoid contamination with catalytically active precious metals. A potentiostat (Autolab, PGSTAT20) was used for potential or current control during the electrochemical measurements. Ultrapure gases, Nitrogen, Oxygen and Hydrogen (BIP plus-X47S, Air products) were used.

S5. Electrochemical performance of gas phase NO poisoned catalysts

Electrochemical measurements of the performance of Fe-N/C and N/C catalyst poisoned in the gas phase using Nitric oxide (see figure 1b in the main paper).

a) Mass transport corrected plot of Fe-CN and C/N catalysts

Mass transport correction of the RDE data was performed using a 4-electron limiting current density of -4.8 mA cm^{-2} and assuming a four electron reaction using

$$i_k = \left(\frac{i\, i_{lim}}{i_{lim} - i}\right)$$

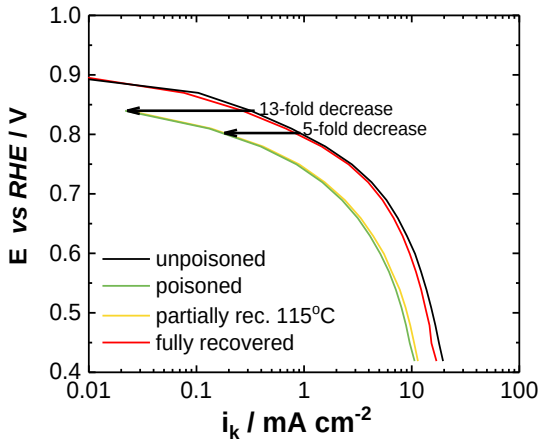

Figure S3 ¦ – Tafel plot of potential versus kinetic current density for data in Figure 1(b) of the main paper. Results obtained from RDE ORR voltammetry of Fe-N/C catalyst in O_2 saturated sulphuric acid before and after poisoning and following recovery. Electrochemical results performed in 0.5 M H_2SO_4, 1600 rpm, 5 mV s^{-1}, loading: 0.26 mg cm^{-2}.

b) Performance towards ORR of C/N catalyst before/after NO treatment

The figure below shows the effect of NO poisoning of N/C catalyst. RDE measurements of pre and post poisoned N/C catalyst. Loading of 0.27 mg cm^{-2}. 0.5M H_2SO_4 electrolyte with a scan rate of 5 mV s^{-1} and a disk rotation rate of 1600 rp.m

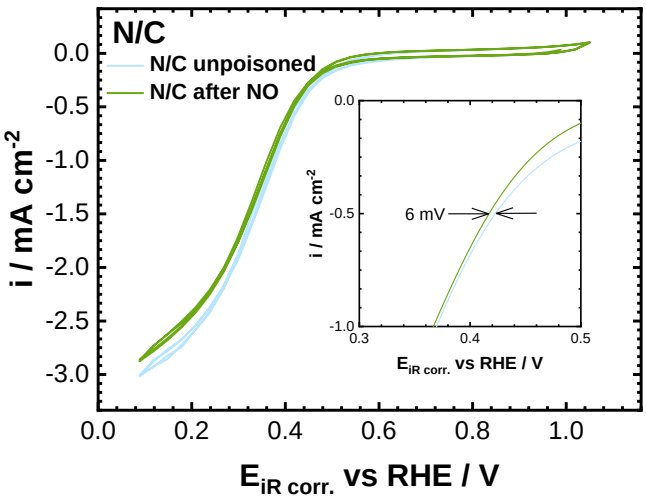

Figure S4 ¦ – RDE ORR voltammetry for nominally iron free N/C catalyst before and after NO exposure. Electrochemical results performed in 0.5 M H_2SO_4, 1600 rpm, 5 mV s^{-1}, loading: 0.26 mg cm^{-2}.

S6. XPS shifts obtained on binding of NO

KB600 shows no response in the N 1s region (figure S5) and no shift in the C 1s peak on adsorption of NO (figure S6)

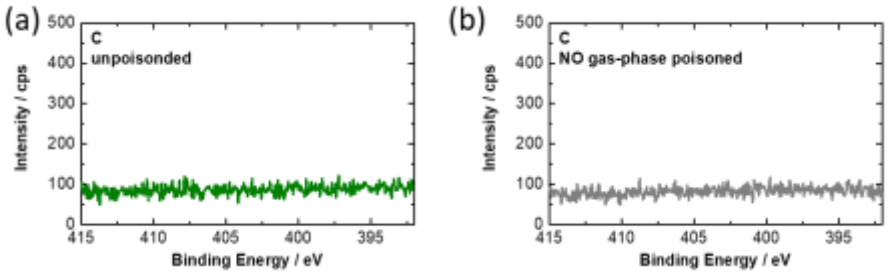

Figure S5 ¦ N 1s fine scan region of KB600 with (left) and without (right) NO adsorption.

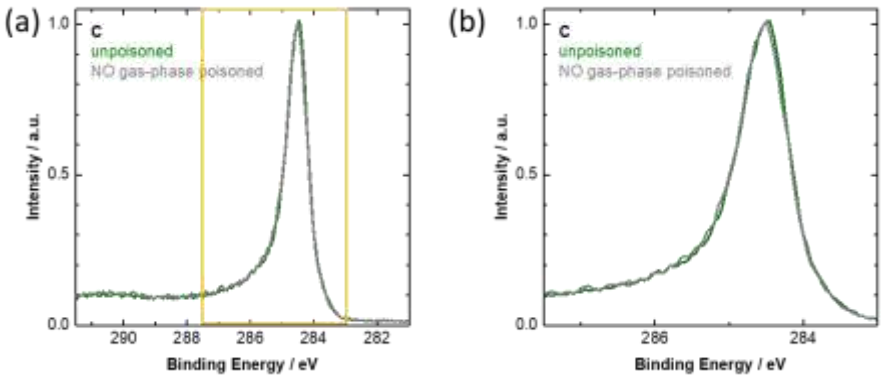

Figure S6 ¦ Influence of NO poisoning treatment on C 1s peak of KB600.

S7. ^{57}Fe Mössbauer Fits and parameters of all catalysts

Details of the fitting parameters and quality of fits are provided in **Table S2** and **Figure S7**

Table S2 ¦ Summary of the Mössbauer parameters and relative absorption areas assigned to iron species. NO poisoned refers to the gas-phase poisoned catalyst. Errors in terms of standard deviation from the measurements of the four samples are given in parenthesis. Individual errors of each sample from fitting (in terms of 95 % confidential intervals) were either smaller or similar.

Mößbauer site		D1	D2	$D3_{Dodelet}$	$D3_{porph}$	Sext1	Sext2
assignment		**N-$Fe^{II}N_4$-X, LS**	**$Fe^{II}N_4$, IS, FePc-type**	**N-$Fe^{II}N_4$, HS**	**$Fe^{II}N_4$, IS, porph-type**	**Iron nitride nanoparticles**	**Troilite FeS**
δ_{iso} / mm s^{-1}		0.381 (0.001)	0.36 (0.03)	1.14 (0.03)	0.38 (0.01)	0.46 (0.01)	0.74 (0.02)
ΔE_Q / mm s^{-1}		1.00 (0.05)	2.91 (0.03)	2.11 (0.06)	1.72 (0.05)	-	-
fwhm / mm s^{-1}		0.78 (0.02)	0.8 (fixed)	0.52 (0.06)	0.8 (fixed)	0.4 (fixed)	0.44 (fixed)
H_0 / T		-	-	-	-	13.31 (0.08)	31.06 (0.03)
Areas / %	unpoisoned	48.3 (1.9)	11.7 (0.3)	6.3 (0.6)	27.6 (1.4)	4.5 (0.2)	1.6 (0.2)
	NO poisoned	48.5 (1.8)	14.5 (0.4)	4.2 (0.6)	26.8 (1.4)	4.6 (0.2)	1.4 (0.2)
	partially rec.	46.3 (1.3)	13.9 (0.3)	5.2 (0.6)	28.2 (1.0)	4.8 (0.2)	1.6 (0.2)
	fully rec.	43.2 (1.3)	11.4 (0.2)	8.0 (0.6)	30.8 (1.0)	5.0 (0.2)	1.6 (0.1)

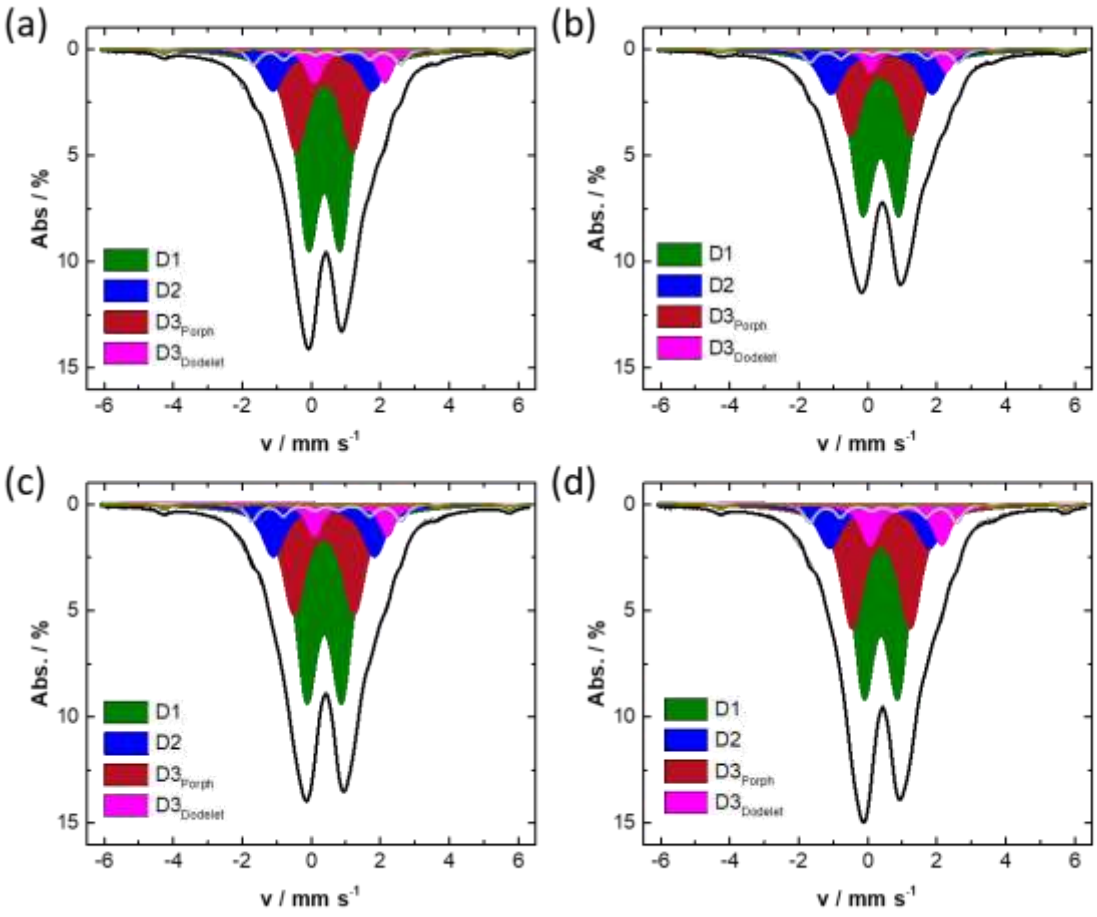

Figure S7 ¦ Fitted Mössbauer spectra of Fe-N/C catalysts: (a) unpoisoned , (b) NO gas-phase poisoned, (c) partial rec. 115 °C and (d) fully recovered.

S8. TPD NO adsorbed on surfaces with O_2 preadsorbed and O_2 adsorbed on surfaces with NO preadsorbed

Two experiments were carried out, one where Fe-N/C was exposed to NO before being exposed to O_2, and one where Fe-N/C was exposed to O_2 before being exposed to NO. Both experiments used similar conditions to other TPD experiments described. In both cases the samples were heat treated in argon at 600 °C as in other experiments, before being cooled and exposed to the first gas for one hour, with a one hour purge with argon before exposure to the second gas. Finally, there is a one hour purge of argon before the TPD experiment, which in both cases is carried out under argon with a heating rate of 20 °C/min.

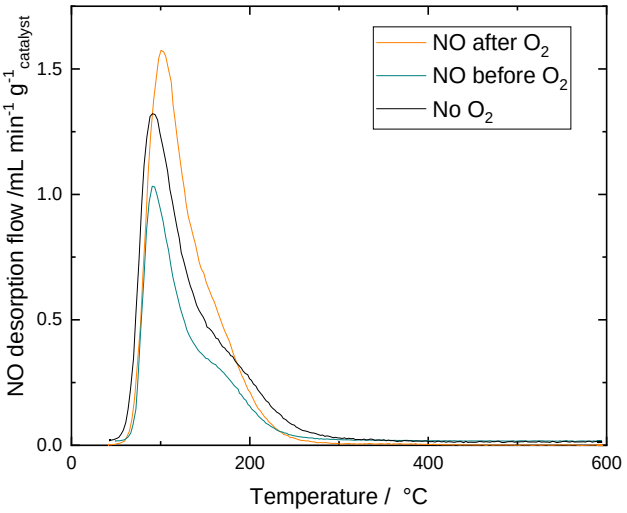

Figure S8 ¦ Effect of oxygen pretreatment on NO adsorption. Temperature programmed desorption curve for NO adsorbed onto Fe-N/C (black), NO adsorbed onto Fe-N/C with O_2 preadsorbed (orange), and NO adsorbed onto Fe-N/C followed by 1 hour of O_2 exposure (cyan)

S9. TPD of oxygen as a function of number of thermal cycles

The cycling experiments were carried out as described below in **Figure S9**. As part of each cycle the sample is heated to 200 or 300 °C and the desorption of gases is measured. With each cycle, the amount of oxygen desorbed as oxygen and CO_2 is measured as the temperature is ramped to the final temperature. **Figure S10** shows the case where oxygen is exposed to the catalyst for only the first and last cycle (i.e. this emasures whether the temperature cycling alone is responsible for the losss in CO_2 emission , whereas the other figures show the effects when oxygen is exposed for each cycle. **Figure S11** and **Figure S12** show oxygen desorbed on cycling to 200 and 300 °C respectively and **Figure S13** for CO_2 desorbed on cycling to 200 °C. CO_2 desorbed on cycling to 300 °C is shown in figure 3b. Because the experiments take several days, calibration is not feasible, so the CO_2 and O_2 mass spectrum peaks are normalised against an Ar peak to obtain values which are stable over time.

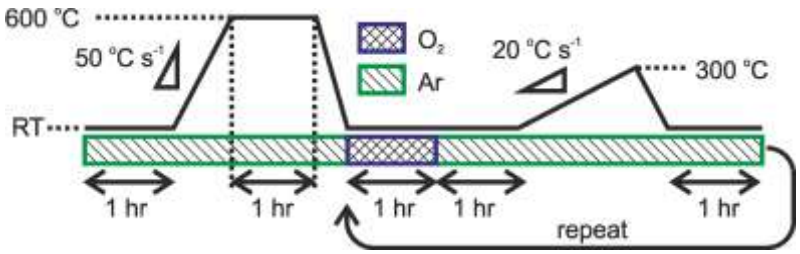

Figure S9 ¦ Procedure for the oxygen cycling experiments.

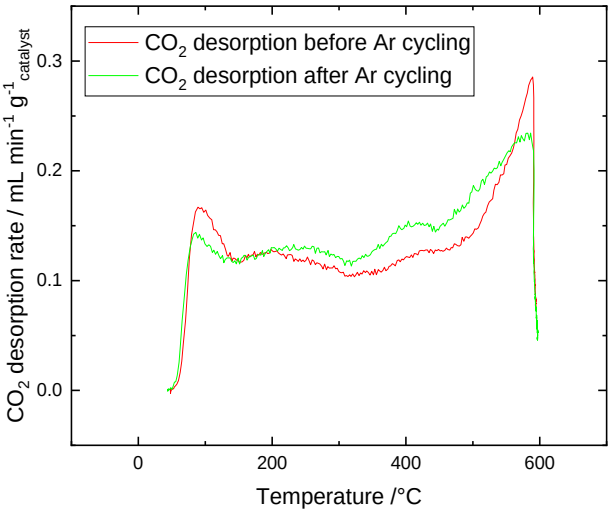

Figure S10 ¦ CO_2 desorption curves after exposure to oxygen before and after 25 cycles to 300 °C in argon.

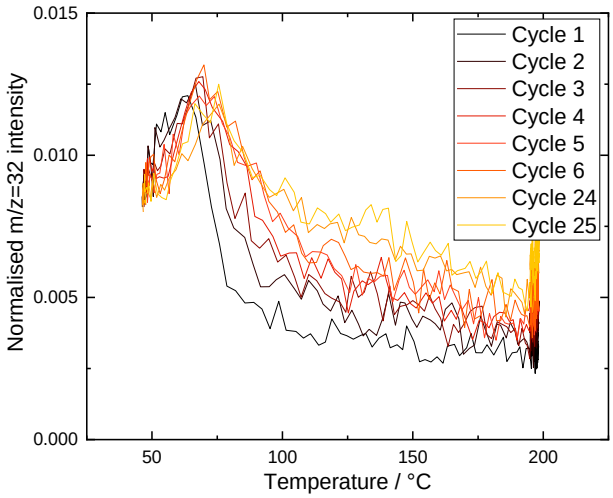

Figure S11 ¦ Oxygen desorption curves on heating to 200 °C in Ar after oxygen adsorption onto Fe-N/C during the oxygen cycling experiments.

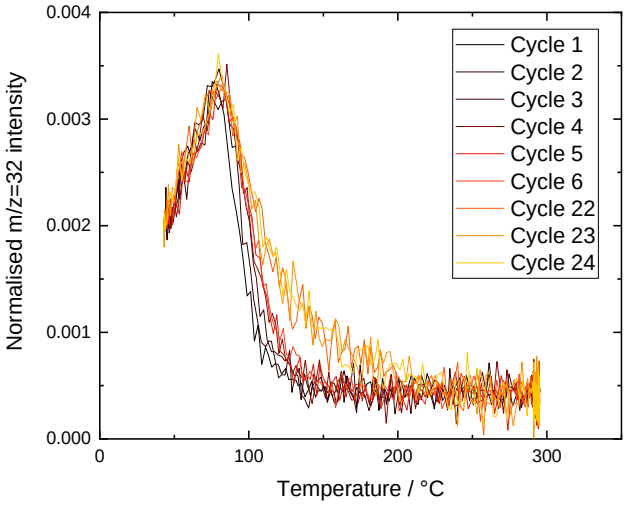

Figure S12 ¦ Oxygen desorption curves on heating to 300 °C after oxygen adsorption onto Fe-N/C during the oxygen cycling experiments.

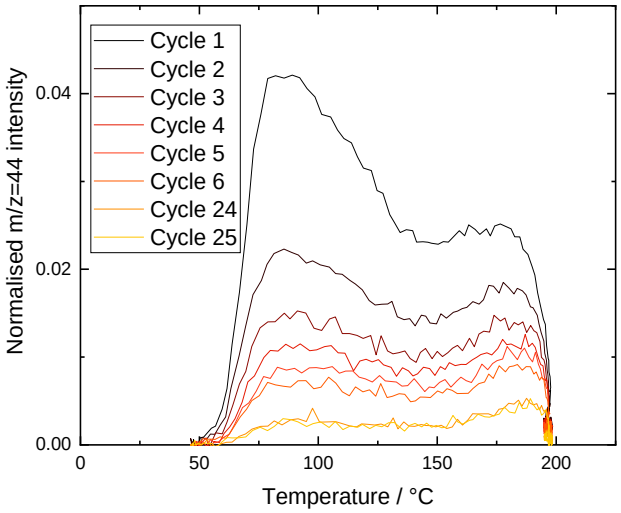

Figure S13 ¦ CO_2 desorption curves on heating to 200 °C after oxygen adsorption onto Fe-N/C during the oxygen cycling experiments.

After the experiments cycling to 300 °C, the sample was heated to 600 °C in argon to measure the amount of CO and CO_2 given off at higher temperatures (**Figure S14**).

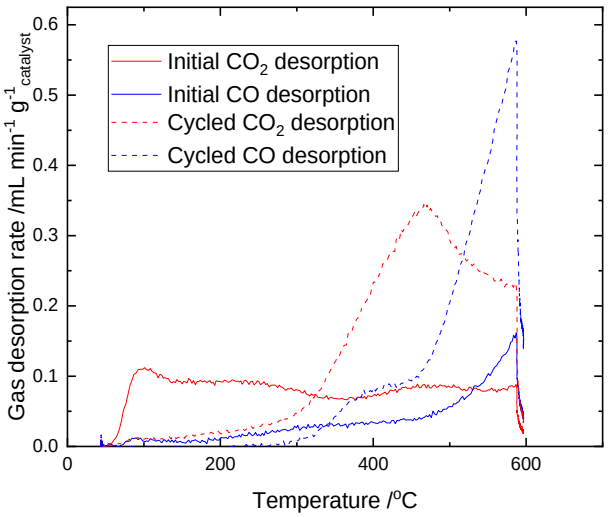

Figure S14 ¦ CO_2 and CO desorption curves on heating to 600 °C.

This sample is then exposed to O_2 for one hour and then heated to 600 °C under argon. The CO_2 and CO desorbed are also shown in **Figure S15**, showing that most of the low temperature CO_2 is recovered by the heat treatment to 600 °C after cycling

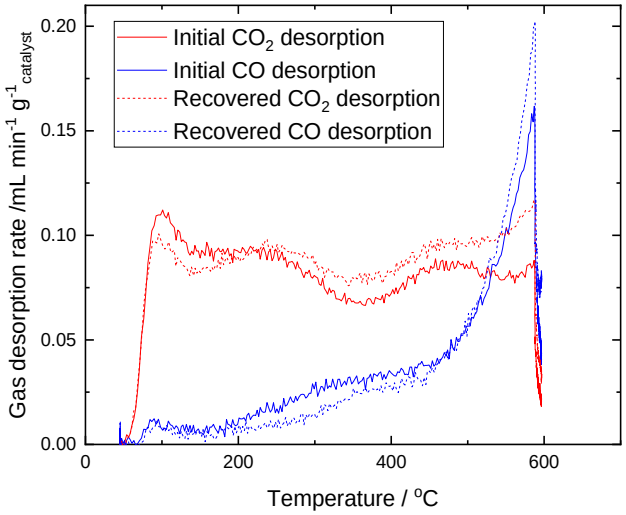

Figure S15 ¦ CO_2 and CO desorption on heating to 600 °C before and after the cycling experiments described in **Figure S9**

S10. BET before and after oxygen treatment

BET analysis of the catalyst immediately after heat treatment at 600 °C in Ar showing the effect of 25x exposure to oxygen followed by ramping the temperature to 300 C under Argon (see Figure 3 of main paper and associated discussion)

Table S3 ¦ Variation of surface area after oxygen and heat treatment

Catalyst	BET SSA ($m^2\ g^{-1}$)	t-plot micropore area ($m^2\ g^{-1}$)	Total pore volume-adsorption ($cm^3\ g^{-1}$)	Total pore volume-desorption ($cm^3\ g^{-1}$)	Micropore volume ($cm^3\ g^{-1}$)
Fe-C/N - 600 C Ar 1 hr	495	435	0.324	0.368	0.173
Fe-C/N O_2 Cycled 25x - 600 C Ar 1 hr	570	493	0.341	0.411	0.196

S11. Kinetic current density for Fe-N/C performance after oxygen thermal treatment and 600°C reset.

Mass transport correction of the RDE data was performed using a 4-electron limiting current density of -4.8 mA cm^{-2} and assuming a four electron reaction using

$$i_k = \left(\frac{i\, i_{lim}}{i_{lim} - i}\right)$$

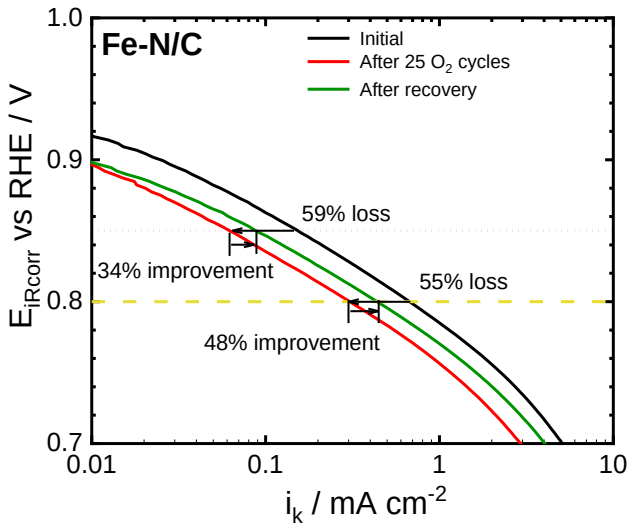

Figure S16 ¦ Tafel plot of potential versus kinetic current density for data in Figure 3(c) of the main paper. Results obtained from RDE ORR voltammetry of Fe-N/C catalyst in O_2 saturated sulphuric acid before and after oxygen adsorption and temperature ramp treatment, and following recovery at 600°C. Electrochemical results performed in 0.5 M H_2SO_4, 1600 rpm, 5 mV s^{-1}, loading: 0.26 mg cm^{-2}.

S12. Fuel Cell performance curve

Below is the non iR corrected fuel cell performance curve of the Fe-N/C catalyst operating on 1 bar(abs) H_2/O_2. Humidity, temperature and gas flow rate were controlled using a Scribner FC test station (850e). Potential and current control were performed using a Gamry Reference 3000 potentiostat. Oxygen (BIP Plus, Air Products) flow rate was 550 mL min^{-1} and hydrogen (BIP Plus, Air Products) flow rate was 150 mL min^{-1} in order to avoid the possibility of oxidant or fuel starvation, while relative humidity was 100% for both gases and cell temperature was maintained at 80°C.

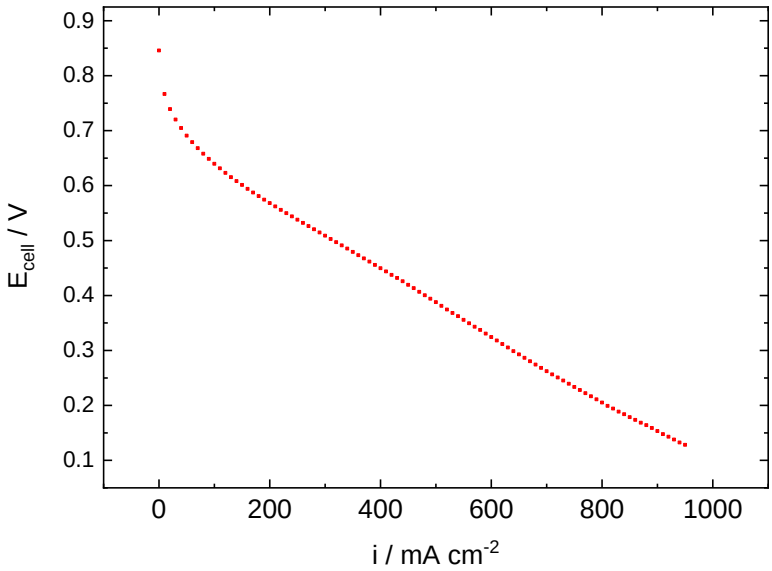

Figure S17 ¦ Fuel cell IV polarisation curve for Fe-N/C catalyst operating in a hydrogen-oxygen fuel cell. Loading of Fe-N/C catalyst 4 $mg_{Fe\text{-}N/C}$ cm^{-2} Results performed at 80°C cell temperature, 100% RH at both anode (pure hydrogen) and cathode (pure oxygen) feed with no backpressure.

S13. Fitting Fuel Cell Transient Data

Initial attempts to fit the transients to simple decay models (e.g. 1st order exponential decays) gave poor results e.g. see below for the fit to

$$i(t) = i(0)exp\left(\frac{-t}{\tau}\right) + i_{offset}$$

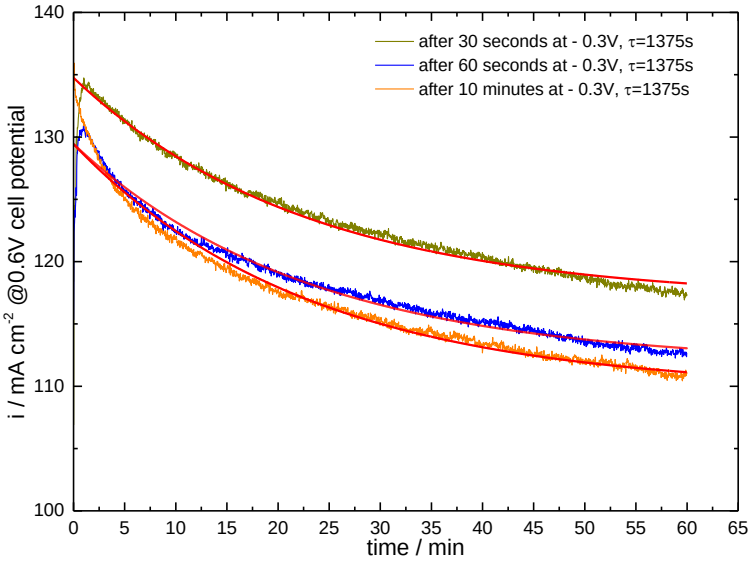

Figure S18 ¦ Chronoamperometric decay curve for Fe-N/C catalyst operating in a hydrogen-oxygen fuel cell at 0.6 V. Loading of Fe-N/C catalyst 4 $mg_{Fe\text{-}N/C}$ cm^{-2} Results performed at 80°C cell temperature, 100% RH at both anode (pre hydrogen) and cathode (pure oxygen) feed. Data is fit to a 1st order exponential decay.

Each of the transients give poor fits when the fits are optimised to use the same time constant (as would be expected for this system) and that the resulting fits would overestimate the current at longer periods. It was realised that the reason for the poor fitting performance was because there was an underlying decay in performance which needed to be taken into account. This decay in performance is seen in the results before the transient experiments started. Thus the decay in performance was incorporated as a slow linear decrease (this is more likely an exponential decrease with a very long time constant, so it appears near enough to being linear during the course of the experiment).

$$i(t) = i(0) - mt$$

Where m is the rate of linear current decay (~1.5 μA cm^{-2} s^{-1}) for the experiments we performed as determined by fitting the linear decay of the results. $i(0)$ is the initial current at the beginning of the experiment. Removing this background linear decrease allowed the exponential decays to all be fit by the same time constant.

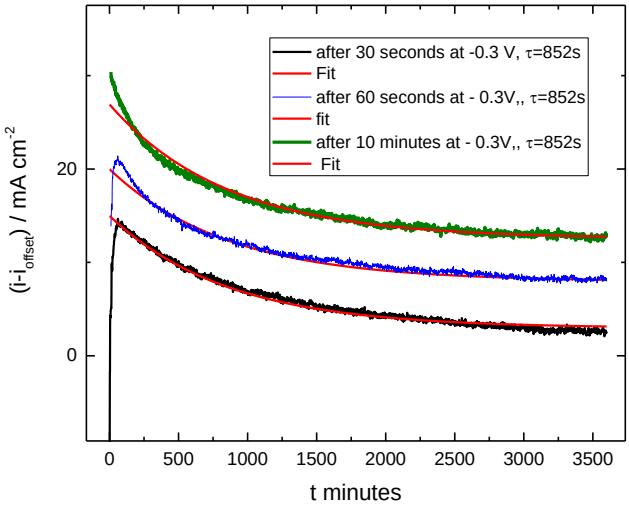

Figure S19 ¦ Chronoamperometric decay curve for data in Figure S18 corrected for a linear decay transient. Data is fit to a 1st order exponential decay

Transients were fit to a 1st order exponential decay superimposed on top of a linear current decrease

$$i(t) = [i(0) - mt] + \left[i_{activation} exp\left(\frac{-t}{\tau}\right) + i_{activation,offset}\right]$$

Where $i_{activation}$ is the maximum current enhancement due to the reductive treatment, τ is the time constant for relaxation back to the background decay rate, $i_{activation,offset}$ is the value of current enhancement due to the treatment at long time. A crucial aspect of using this approach is that all three curves can be fit with same time constant of decay (τ) to give reasonable fits.

The above formula is functionally equivalent to

$$i(t) = \left[i(0) - m\left(t - t_{offset}\right)\right] + i_{activation} exp\left(\frac{-t}{\tau}\right)$$

t_{offset} is related to $i_{activation,offset}$ by

$$t_{offset} = \frac{i_{activation,offset}}{m}$$

In the absence of any transient, the current slowly decays at a rate which approximates a linear decay. After the reductive potential treatment, the current increases, but shows a first order decay back towards the same linear decay as was previously seen. However, that background decay is at a higher level than was previously seen, but still has the same slope. That longterm effect is equivalent to the fuel cell operating at an earlier time (and thus higher

current), given by t_{offset}. In our experiments, t_{offset} is of the order of ~2 hours i.e the short reductive treatment is equivalent to giving the fuel cell two more hours of lifespan.

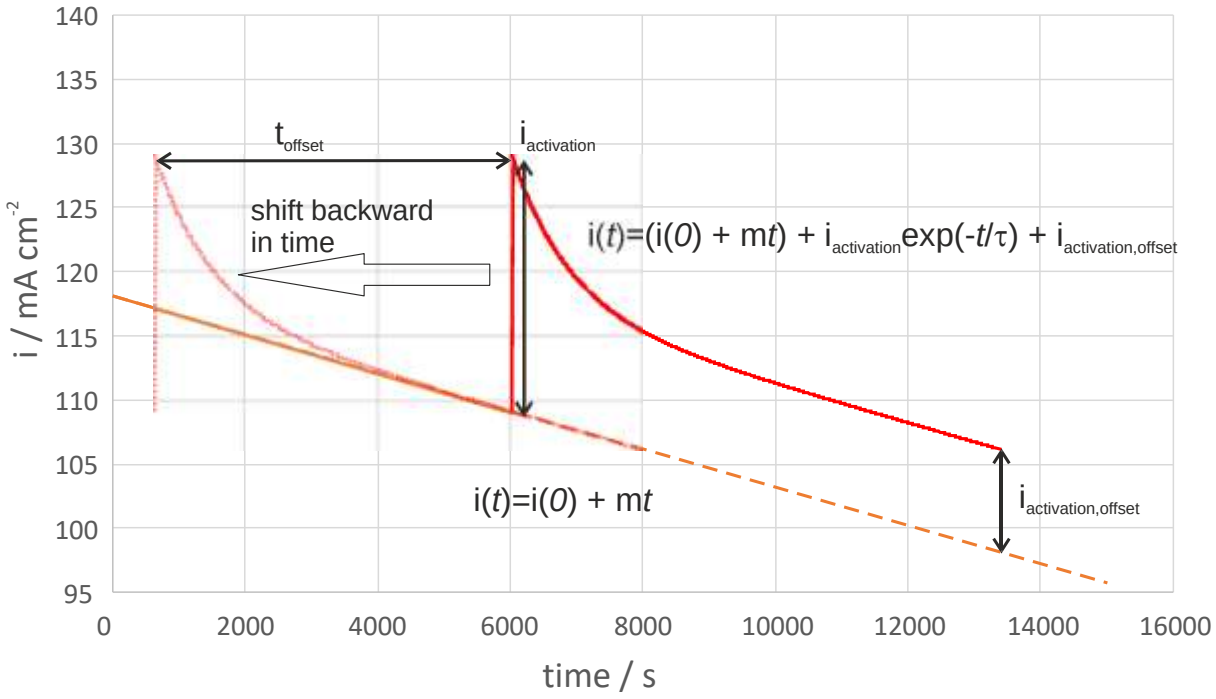

Figure S20 ¦ Cartoon showing form of chronoamperometric decay and how the reactivation process is equivalent to a backwards time shift.

Fitting was accomplished in Excel using Solver and the GRG Nonlinear method using Multistart in order to assure that the global best fit parameters were found. All transients were fit with the same timeconstant, but with different values of $i_{activation}$ and $i_{activation,offset}$. The linear decay of current with time was taken into account using the value of *m* discussed above. The first 15 seconds were not fit as the currents were skewed by double layer charging transients and contributed to half of the error in fitting the transients.

Table S4 ¦ Results for the fitting of the transients and also the integration of the current

Parameter	Transient based on length of time at -0.3 V		
	1 (30s)	2 (60s)	3 (300s)
$i_{activation,offset}$ / mA cm^{-2}	8.0	8.2	12.1
τ / s	840		
$i_{activation}$ / mA cm^{-2}	12.2	12.3	14.4
t_{offset} / s	5340	5470	8150
Q_{total} / C cm^{-2}	443	425	420
$Q_{linear\ decay}$ / C cm^{-2}	405	386	364
Q_{Extra} / C cm^{-2}	38	39	56
Q_{Extra}/ $Q_{linear\ decay}$	9.5%	10.2%	15.3%

References

1. J.-Y. Choi, R. S. Hsu and Z. Chen, *The Journal of Physical Chemistry C*, 2010, **114**, 8048-8053.
2. D. Holmes Parker, M. E. Jones and B. E. Koel, *Surface Science*, 1990, **233**, 65-73.
3. U. A. Paulus, T. J. Schmidt, H. A. Gasteiger and R. J. Behm, *Journal of Electroanalytical Chemistry*, 2001, **495**, 134-145.
4. T. J. Schmidt, H. A. Gasteiger, G. D. Stäb, P. M. Urban, D. M. Kolb and R. J. Behm, *Journal of The Electrochemical Society*, 1998, **145**, 2354-2358.